

Local Susceptibility of the $\text{Yb}_2\text{Ti}_2\text{O}_7$ Rare Earth Pyrochlore Computed from a Hamiltonian with Anisotropic Exchange

J D Thompson¹, P A McClarty¹, and M J P Gingras^{1,2}

¹Department of Physics and Astronomy, University of Waterloo, Waterloo, ON, N2L 3G1, Canada.

²Canadian Institute for Advanced Research, 180 Dundas Street West, Toronto, Ontario M5G 1Z8, Canada

Abstract. The rare earth pyrochlore magnet $\text{Yb}_2\text{Ti}_2\text{O}_7$ is among a handful of materials that apparently exhibit no long range order down to the lowest explored temperatures and well below the Curie-Weiss temperature. Paramagnetic neutron scattering on a single crystal sample has revealed the presence of anisotropic correlations and recent work has led to the proposal of a detailed microscopic Hamiltonian for this material involving significantly anisotropic exchange. In this article, we compute the local sublattice susceptibility of $\text{Yb}_2\text{Ti}_2\text{O}_7$ from the proposed model and compare with the measurements of Cao and coworkers [8], finding quite good agreement. In contrast, a model with only isotropic exchange and long range magnetostatic dipoles gives rise to a local susceptibility that is inconsistent with the data.

1. Introduction

The pyrochlore lattice of corner-sharing tetrahedra is a classic example of a lattice prone to geometric frustration, the inability of interacting magnetic moments on such a lattice to simultaneously minimize all of the pairwise interactions in the system. In the rare earth oxides, $A_2B_2O_7$, where A is a trivalent rare earth ion (Ho, Dy, Tb, Gd, Yb) or yttrium (Y) and B is a tetravalent transition metal ion (Ti, Sn, Mo, Mn), both A and B reside on distinct interpenetrating pyrochlore lattices. Such systems have been the subject of intense research for the past 10 years as they are known to manifest a wide variety of exciting collective phenomena [1] including spin ices ($\text{Dy}_2\text{Ti}_2\text{O}_7$, $\text{Ho}_2\text{Ti}_2\text{O}_7$) [2], spin liquids ($\text{Tb}_2\text{Ti}_2\text{O}_7$) [3], spin glasses ($\text{Y}_2\text{Mo}_2\text{O}_7$) [4], and LRO with persistent spin dynamics ($\text{Gd}_2\text{Sn}_2\text{O}_7$, $\text{Er}_2\text{Ti}_2\text{O}_7$) [5, 6].

To better understand the many complex phenomena observed in magnetic pyrochlore oxides, knowledge of the microscopic interactions present in these materials is necessary. The pyrochlore lattice can be described as an FCC Bravais lattice with a tetrahedral basis at each FCC site. The magnetic rare earth (A^{3+}) ions reside on the pyrochlore lattice and are subject to a crystal field (CF) which introduces a

magnetic anisotropy with respect to the local $\langle 111 \rangle$ axes that is reflected in the magnetic susceptibility on each of the four sublattices. Recently, determination of the local susceptibility, χ_a , via polarized neutron scattering has been brought to bear on the rare earth pyrochlores including $\text{Tb}_2\text{Ti}_2\text{O}_7$, $\text{Ho}_2\text{Ti}_2\text{O}_7$, $\text{Er}_2\text{Ti}_2\text{O}_7$, and $\text{Yb}_2\text{Ti}_2\text{O}_7$ [8]. These measurements have been used to analyse the single ion anisotropy and the nature of the magnetic interactions [8, 9]. In particular, despite concerns about some details of the method with which the theoretical analysis of χ_a is carried out in Refs. [8, 9], which we discuss later on in the Appendix, both of these works arrive at the tentative conclusion that in most of these materials, isotropic exchange interactions are inadequate to account for the χ_a measurements and that, instead, the interactions appear to some extent anisotropic. The presence of anisotropic exchange in the pyrochlore oxides provides a further clue to the vehicle for the richness of phenomena observed in rare earth frustrated magnets [1]. Indeed, recent theoretical work has exposed large anisotropic superexchange in pyrochlore oxide materials [10, 11].

In this paper, we focus on local susceptibility measurements on one material, $\text{Yb}_2\text{Ti}_2\text{O}_7$ [8], which is remarkable for exhibiting a phase transition at $T_c \approx 240$ mK, albeit with no signs of long range magnetic order at lower temperatures [12]. The nature of the low temperature phase in $\text{Yb}_2\text{Ti}_2\text{O}_7$ is currently somewhat controversial. Reference [13] reports the onset of hysteresis in the vicinity of 240 mK and the presence of magnetic Bragg peaks at lower temperatures. Other studies, however, have found no evidence of magnetic reflections [12, 14, 15] in zero applied field. Reference [12] presents muon spin relaxation data revealing that the spin fluctuation rate drops sharply at about 240 mK, but remains nonzero and temperature independent well below T_c , perhaps indicating a spin gas to spin liquid type phase transition. Peculiarly, the collective paramagnetic state exhibits strongly anisotropic rod-like correlations in the diffuse neutron scattering which have been conjectured to arise from a weak decoupling of the kagome layers in the pyrochlore lattice [15]. We have investigated the origin of the correlations seen in neutron scattering by using a random phase approximation calculation of the paramagnetic neutron scattering intensity pattern and found a set of interactions that produce a theoretical scattering pattern that is in very good agreement with the experimental data [16]. The foremost characteristic of these interactions is that they are strongly anisotropic. The purposes of the present work are (i) to provide a comparison of the predictions of our microscopic Hamiltonian [16] with the local susceptibility (χ_a) data of Ref. [8] and (ii) to provide a discussion of the sensitivity of χ_a to the nature of the interactions and compare with the results of Refs. [8] and [9]. We show that our model can successfully account for the observed temperature dependence of χ_a without further adjustment to the exchange couplings determined in Ref. [16].

2. Anisotropic Exchange Model

In this section, we provide a description of a candidate theory for the magnetism of $\text{Yb}_2\text{Ti}_2\text{O}_7$ introduced in Ref. [16]. The magnetic Yb^{3+} ion has electronic configuration

$^2\text{F}_{7/2}$, such that $J = 7/2$ and Landé factor $g_J = 8/7$. The nearest neighbour distance between Yb^{3+} ions is $r_{\text{nn}} = (a/4)\sqrt{2}$, where $a = 10.026 \text{ \AA}$ is the size of the conventional cubic unit cell [14]. The single ion crystal field interaction H_{cf} is the largest magnetic energy scale. The form of H_{cf} is fixed by the symmetry of the Yb^{3+} environment. To specify H_{cf} completely, we require the values of the six crystal field (CF) parameters. We use two independent sets of CF parameters determined in Refs. [8, 17]. The magnetic Hamiltonian is $H = H_{\text{cf}} + H_{\text{int}}$, which includes both the CF and spin-spin interactions of the form $H_{\text{int}} = H_{\text{ex}} + H_{\text{dip}}$ which is composed of exchange, H_{ex} , and long range magnetostatic dipolar interactions $H_{\text{dip}} = \sum_{i>j;a,b} \frac{D(r_{\text{nn}})^3}{|\mathbf{R}_{ij}^{ab}|^3} [\mathbf{J}_i^a \cdot \mathbf{J}_j^b - 3(\mathbf{J}_i^a \cdot \hat{\mathbf{R}}_{ij}^{ab})(\mathbf{J}_j^b \cdot \hat{\mathbf{R}}_{ij}^{ab})]$ with coupling $D = \frac{\mu_0(g_J\mu_B)^2}{4\pi r_{\text{nn}}^3} \approx 0.01848 \text{ K}$. H_{ex} contains all nearest neighbour exchange interactions, \mathcal{J}_e , that respect lattice symmetries. There are four such nearest neighbour interactions [18]: $H_{\text{Ising}} = -\mathcal{J}_{\text{Ising}} \sum_{\langle i,j \rangle; a,b} (\mathbf{J}_i^a \cdot \hat{\mathbf{z}}^a) (\mathbf{J}_j^b \cdot \hat{\mathbf{z}}^b)$, which couples the local [111] $\hat{\mathbf{z}}$ components of \mathbf{J} (shown in Fig. 1(a)), $H_{\text{iso}} = -\mathcal{J}_{\text{iso}} \sum_{\langle i,j \rangle; a,b} \mathbf{J}_i^a \cdot \mathbf{J}_j^b$, the standard isotropic exchange, $H_{\text{pd}} = -\mathcal{J}_{\text{pd}} \sum_{\langle i,j \rangle; a,b} [\mathbf{J}_i^a \cdot \mathbf{J}_j^b - 3(\mathbf{J}_i^a \cdot \hat{\mathbf{R}}_{ij}^{ab})(\mathbf{J}_j^b \cdot \hat{\mathbf{R}}_{ij}^{ab})]$, a pseudo-dipolar interaction of exchange origin and not part of H_{dip} and, finally, $H_{\text{DM}} = -\mathcal{J}_{\text{DM}} \sum_{\langle i,j \rangle; a,b} \boldsymbol{\Omega}_{\text{DM}}^{a,b} \cdot (\mathbf{J}_i^a \times \mathbf{J}_j^b)$, the Dzyaloshinskii-Moriya (DM) interaction [19]. In all of these terms, \mathbf{J}_i^a denotes the angular momentum of the Yb^{3+} located at lattice \mathbf{R}_i^a (FCC lattice site i and tetrahedral sublattice site a) and $\hat{\mathbf{R}}_{ij}^{ab}$ is a unit vector directed along $\mathbf{R}_j^b - \mathbf{R}_i^a$.

In our recent work [16], we were able to determine the values of $\mathcal{J}_e \equiv \{\mathcal{J}_{\text{iso}}, \mathcal{J}_{\text{Ising}}, \mathcal{J}_{\text{pd}}, \mathcal{J}_{\text{DM}}\}$. We accomplished this by fitting the diffuse paramagnetic neutron scattering measurements to neutron scattering patterns generated using the random phase approximation [16]. The fitting was done by treating the four exchange couplings, \mathcal{J}_e , as free parameters, and determining their optimal values using simulated annealing to minimize the difference between the model and experimental scattering patterns, along with a term to fix θ_{CW} to the value reported in Ref. [17] of $\theta_{\text{CW}} = 0.75 \text{ K}$ [20]. The values of \mathcal{J}_e we extracted are [16]:

$$\mathcal{J}_{\text{Ising}} = 0.81 \text{ K} \quad \mathcal{J}_{\text{iso}} = 0.22 \text{ K} \quad \mathcal{J}_{\text{pd}} = -0.29 \text{ K} \quad \mathcal{J}_{\text{DM}} = -0.27 \text{ K} \quad (1)$$

when using the CF parameters of [17], and

$$\mathcal{J}_{\text{Ising}} = 0.76 \text{ K} \quad \mathcal{J}_{\text{iso}} = 0.18 \text{ K} \quad \mathcal{J}_{\text{pd}} = -0.26 \text{ K} \quad \mathcal{J}_{\text{DM}} = -0.25 \text{ K} \quad (2)$$

when using the CF parameters of [8]. The values of \mathcal{J}_{DM} in both of these sets of interactions are large, even compared to values found in other insulating pyrochlore materials based on magnetic d-shell transition metal ions that display significant DM interactions [21, 22]. However, it has recently been shown that large DM interactions are allowed in $\text{Yb}_2\text{Ti}_2\text{O}_7$ due to antisymmetric contributions to the superexchange between Yb^{3+} ions mediated via the oxygen ions at the O1 site (i.e. in the middle of each tetrahedron) [11].

3. Local Susceptibility

We briefly outline the method of Gukasov and Brown [23] for determining the components of the site susceptibility tensor from polarized neutron scattering. In the presence of a magnetic field, the induced moment on sublattice a at fcc site \mathbf{R}_i is given by $\mathbf{M}_a(\mathbf{R}_i)$ where we assume that there is no contamination from $\mathbf{k} \neq 0$ magnetic structures. The magnetic Bragg intensity $I(\mathbf{q})$ depends on $\mathbf{M}(\mathbf{q})$, the magnetic moment in reciprocal space, and is given by

$$I(\mathbf{q}) \propto \left(\sum_{\mathbf{G}} \delta(\mathbf{q} - \mathbf{G}) \right) \left(\bar{b}^2 + \bar{b}\mathbf{P}_0 \cdot \mathbf{T}(\mathbf{q}) + \frac{1}{4}\mathbf{T}(\mathbf{q}) \cdot \mathbf{T}(\mathbf{q}) \right)$$

where $\mathbf{T}(\mathbf{q}) = \frac{1}{2}aF(\mathbf{q})[\mathbf{M}(\mathbf{q}) - \hat{\mathbf{q}}(\mathbf{M}(\mathbf{q}) \cdot \hat{\mathbf{q}})]$ and both \bar{b} and a are constants. Since the neutron intensity depends on the neutron polarization vector \mathbf{P}_0 , measurements of the spin-non-flip and spin-flip intensity for different Bragg peaks provide information about the moments on each sublattice.

The site susceptibility χ_a is defined as $M_a^\alpha(\mathbf{R}_i) = \bar{\chi}_a^{\alpha\beta} h^\beta$ where h^β is the applied magnetic field and α, β are components in the crystallographic frame, with the bar over χ_a indicating the choice of the crystallographic frame. In the refinement of the moments from the neutron data, $\bar{\chi}_a$ on sublattice 1 (at the fcc sites) was taken to have two components with all diagonal elements equal and all off-diagonal elements equal in the crystallographic frame. In the experiment [8] on $\text{Yb}_2\text{Ti}_2\text{O}_7$, the applied magnetic field was 1 T in the [110] direction, so the experiment was sensitive to components $\bar{\chi}_1^{\alpha\beta}$ with $\alpha = 1, 2$. Figure 1(a) shows the tetrahedral basis with the choice of sublattice labelling as well as the local Ising $\langle 111 \rangle$ directions and the [110] orientation of the applied magnetic field.

We computed the moments and hence the site susceptibility within a local mean field theory by computing the single ion spectra self-consistently in the presence of a magnetic field. Each bilinear spin operator $J_i^\alpha J_j^\beta$, with spin components α and β , in the interaction Hamiltonian H_{int} was written as

$$J_i^\alpha J_j^\beta \rightarrow J_i^\alpha \langle J_j^\beta \rangle + \langle J_i^\alpha \rangle J_j^\beta - \langle J_i^\alpha \rangle \langle J_j^\beta \rangle + (J_i^\alpha - \langle J_i^\alpha \rangle) (J_j^\beta - \langle J_j^\beta \rangle)$$

and the last term on the right-hand side - the fluctuation term - was dropped to obtain a decoupled mean field Hamiltonian $H_{\text{int,MF}} \equiv \sum_i H_{\text{int,MF}}(i)$ for each site i . The single ion wavefunctions $|\nu\rangle$, at site i , were obtained from $H_{\text{MF}} \equiv H_{\text{cf}} + H_Z + H_{\text{int,MF}}$ [8, 12] where H_Z is the Zeeman interaction term, $H_Z = -\mu_B g_J \sum_i \mathbf{J}_i^\alpha \cdot \mathbf{B}$ by solving for the moments $\langle J_i^\alpha \rangle$. The infinite lattice sum of the dipolar interaction was computed using Ewald summation [24]. From a set of randomly chosen initial moments, H_{MF} was diagonalized on each site of a cubic unit cell with periodic boundary conditions and the resulting spectrum, $|\nu, i\rangle$, for sites $i = 1, \dots, 16$ and $\nu = 1, \dots, 2J + 1$ used to obtain a new set of moments $\langle J_i^\alpha \rangle = Z^{-1} \text{Tr} \{ J_i^\alpha \exp(-\beta H_{\text{MF}}(i)) \}$ where $Z = \text{Tr} \{ \exp(-\beta H_{\text{MF}}(i)) \}$. The process of successive diagonalization and computation of the moments was iterated until convergence was reached. The process was repeated for each temperature. The use of a single cubic unit cell for the diagonalization is more than sufficient since it was found in

Ref. [16] that the interaction Hamiltonian H_{int} with parameters from either Eq. 1 or 2 leads to $q = 0$ ordering, signifying an identical moment configuration on each tetrahedral primitive unit cell.

From the moments obtained within MF theory, we computed the single ion susceptibility χ_a for each sublattice $a = 1, 2, 3, 4$ - each independent (primitive) tetrahedron being identical. In common with Refs. [8, 9], we present components of the susceptibility parallel (χ_{\parallel}) and perpendicular (χ_{\perp}) to the local Ising directions. These components were computed by introducing rotation matrices $u_a^{\alpha\beta}$ from the global to the local frame with \hat{z}_a axes along the $\langle 111 \rangle$ directions. Transforming $\bar{\chi}_a$ to the local frame $\chi_a^{\alpha\beta} = u_a^{\alpha\gamma} u_a^{\beta\delta} \bar{\chi}_a^{\gamma\delta}$, we extract $\chi_{a,\parallel} \equiv \chi_a^{zz}$. Our choice of local frame is such that the [110] field has vanishing local y component for sublattices 1 and 2 (along the α chains) and vanishing local x and z components for sublattices 3 and 4 (along the β chains). Hence, for sublattices 1 and 2, with an applied [110] field, we take $\chi_{a,\perp} = \chi^{xx}$ and for sublattices 3 and 4, $\chi_{a,\perp} = \chi^{yy}$.

4. Results

Fig. 1(b) shows the single ion $\chi_a = \{\chi_{\parallel}, \chi_{\perp}\}$, computed only from the Zeeman term and CF Hamiltonian using the CF parameters of Refs. [8, 17], and the experimentally determined values of χ_a [8]. Both sets of CF parameters give rise to a χ_{\perp} that fits the experimental data well over the whole temperature range even in the absence of interactions except for the lowest temperature point, $T = 2$ K, where the experimental χ_{\perp} falls below the crystal field prediction. However, the χ_{\parallel} calculations for the two sets of CF parameters are significantly different from one another and from the experiment. Whereas, the parameters of Ref. [8] give a χ_{\parallel} that fits reasonably well between 20 K and 70 K, deviating from experiment at the highest and lowest measured temperatures, those of Ref. [17] do not fit well over most of the temperature range. The addition of anisotropic exchange of the form given in Eq. (1), does not improve the fit to experiment of χ_{\parallel} computed using the CF parameters of Ref. [17]. Because of the poor fit to χ_{\parallel} , even when anisotropic exchange is included, we do not use the CF parameters of Ref. [17] any further in this work despite their fair success in reproducing paramagnetic neutron scattering measurements in Ref. [16]. Another point to be drawn from Fig. 1(b) is that there is a difference between the local susceptibilities for the α and β chains. In particular, χ_{\parallel} is not probed for the 3 and 4 sublattices because the [110] field does not induce a moment in the local [111] Ising direction on these sublattices. Also, χ_{\perp} , which is probed on all four sublattices, is different for the α and β chains. As the temperature is raised, the cubic symmetry between different sublattices is partially restored.

When interactions are included in the computation of χ_a as described in Section 3, we obtain the results shown in Fig. 2. Figure 2(a) shows the local susceptibility, computed for two different models over the temperature range 2 K to 300 K, together with the experimental data of Ref. [8]. The inclusion of interactions does not significantly affect χ_{\perp} so, for these results, we merely observe that the splitting between α and β

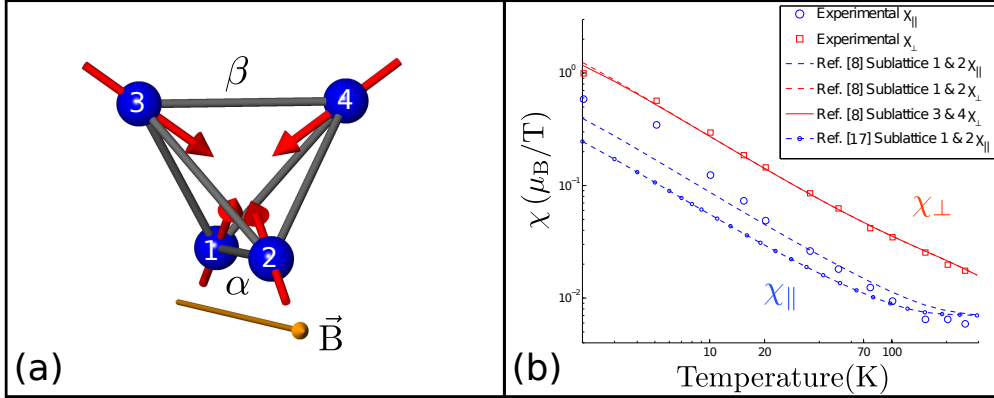


Figure 1. (a) Tetrahedral basis of the pyrochlore structure showing the four anisotropy axes as red arrows and the applied magnetic field \mathbf{B} orientation (orange arrow). Sublattices 1 and 2 make up the α chains and sublattices 3 and 4, the β chains. (b) Local susceptibility (open symbols) as reported in Ref. [8] in a 1 T field along [110], along with single ion local susceptibilities computed using the crystal fields of Ref. [8] (dashed and solid lines) and Ref. [17] (dot-dash line - the perpendicular part having been omitted as it almost coincides with the Ref. [8] crystal field result) in the same field, but without including the \mathcal{J}_e exchange interactions.

chains is present once again because of the symmetry breaking field. The first model to be compared with the experimental χ_{\parallel} data is one with long ranged dipoles and purely isotropic exchange ($\mathcal{J}_{\text{sing}} = \mathcal{J}_{\text{pd}} = \mathcal{J}_{\text{DM}} = 0$), with a coupling $\mathcal{J}_{\text{iso}} = -0.06$ K constrained by the Curie-Weiss temperature which is taken to be $\theta_{\text{CW}} = 0.75$ K, within the experimental error margins given above [16] (blue dot-dash line). The second model is the candidate anisotropic exchange model described in Section 2 and Ref. [16] (blue dashed line). The χ_{\perp} results (red lines) do not strongly distinguish between the two models. At low temperatures, $T \lesssim 30$ K, where the effect of interactions produces significant deviations of χ_{\parallel} from the noninteracting case, the isotropic exchange model does not fit the experimental data as well as the anisotropic exchange model, except at the lowest temperature point (2 K). However, neither model captures the 2 K point for χ_{\perp} .

Fig. 2(b) shows once again the experimental data and the anisotropic model predictions for χ_a as well as χ_a computed using the molecular field method of Ref. [8]. The fit in Ref. [8] of χ_{\parallel} is only provided down to approximately 3.5 K in that work (and no results for χ_{\perp} for the single ion mean field case are reported in that reference). For the temperature range over which the models can be compared, our anisotropic exchange model describes the experimental data as well as the model of Ref. [8]. However, our model achieves this while correctly preserving lattice symmetries, unlike the model of Ref. [8], and therefore corresponds to a physically acceptable microscopic model. We discuss further the comparison of our results with those of Refs. [8, 9] in the Appendix.

At temperatures $T \gg \theta_{\text{CW}}$, interactions are expected to have little effect on χ_a which is borne out by our calculations. Therefore the differences between the

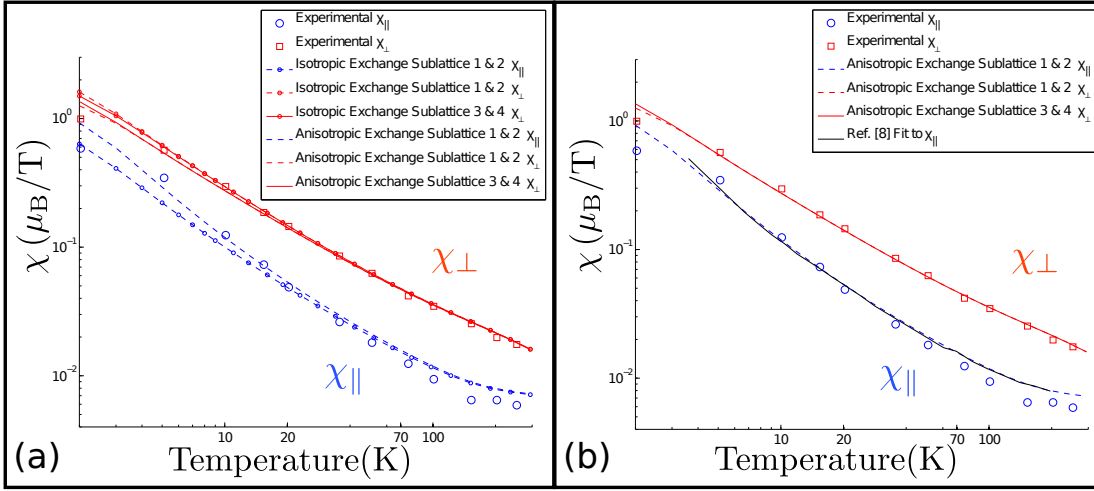


Figure 2. (a): χ_a as reported by [8] (open squares and circles). Also shown is χ_a , for all four magnetically inequivalent sublattices, computed within local mean field theory with our anisotropic exchange model with long range dipoles obtained from neutron scattering data in Ref. [16]. The temperature range is 2 K to 300 K. Also shown is the prediction of a model with isotropic exchange interactions and long ranged dipoles. (b): A comparison of our anisotropic exchange model with the prediction of the model of Ref. [8].

χ_a calculations and experimental results at high temperatures ($T > 100$ K) can be attributed to an incorrect spectral decomposition of the excited crystal field states [8, 17].

5. Discussion

We have investigated the local susceptibility computed from the anisotropic exchange model described in Section 2 for $\text{Yb}_2\text{Ti}_2\text{O}_7$. The model was obtained from an *independent* previous fit to the paramagnetic neutron scattering [16]. The calculations presented here fit the χ_a experimental data well with no adjustable parameters over much of the experimental temperature range (2 K to 250) K. There are, however, discrepancies in the fit above approximately 100 K, presumably due to the fact that the available CF parameters do not capture the correct wavefunctions for the excited CF energy levels. The fit is also imperfect at the lowest observed temperature of 2 K where the experimental χ_a susceptibility flattens out while it does not in the mean field treatment of the Hamiltonian $H = H_{\text{cf}} + H_{\text{int}} + H_{\text{Z}}$.

At high temperatures $T \gg \theta_{\text{CW}}$, χ_a is insensitive to the interactions and the quality of fit is determined by the CF Hamiltonian and the Zeeman term. Fig. 1 illustrates that the crystal field provides an adequate fit to χ_{\parallel} from 100 K down to about 30 K and to χ_{\perp} over the entire range of temperatures. Figure 2 shows that the quality of fit for $T > 30$ K does not change with the inclusion of interactions. Therefore, the only nontrivial test of our model comes from the five lowest temperature points ($T = 2$ K, 5 K, 10 K, 15 K, 20 K) in χ_{\parallel} where the noninteracting Hamiltonian, $H = H_{\text{cf}} + H_{\text{Z}}$,

gives a χ_{\parallel} that falls significantly below the experimental result (see Fig. 1(b)). The anisotropic exchange model determined in Ref. [16] provides a good description of χ_{\parallel} , whereas isotropic exchange interactions do not – this is the main conclusion of this work. Although the relevant test of our model comes from only a few (five) data points, it achieves the goals of providing a *consistency check* of our model determined previously on the basis of diffuse paramagnetic neutron scattering [16] while also establishing that anisotropy in the exchange is indeed an intrinsic ingredient of the spin Hamiltonian of $\text{Yb}_2\text{Ti}_2\text{O}_7$.

Refs. [8] and [9] both extract exchange parameters from the local susceptibility data, and present fits to the local susceptibility that result from these exchange parameters. As stated above, we find that this method for extracting exchange parameters is under constrained. In the Appendix, we describe in some detail the approaches taken in these two papers and compare with our own results.

6. Conclusion

In this work we have shown that the anisotropic exchange model extracted from neutron scattering measurements in a previous work [16] produces a good fit to both local and bulk susceptibility measurements on the rare earth pyrochlore material $\text{Yb}_2\text{Ti}_2\text{O}_7$ for temperatures in the range $T \lesssim 100$ K. This model has four nonadjustable and a priori prescribed bilinear exchange couplings which were extracted from neutron scattering data [16]. The fit of our model to the experimental measurements of χ_a and the bulk susceptibility provides further *independent* evidence for the correctness of our anisotropic exchange model [16].

We also found that the origin of the discrepancy between the experiment and our model at high temperatures, and indirectly, a similar failure to fit the local susceptibility χ_a also at $T \gtrsim 10^2$ K in Ref. [8], lies in the excited CF states obtained from the CF parameters of Refs. [8, 17]. Further experimental work would be required to probe more accurately the spectral decomposition of the excited states of the crystal field in order to better determine their structure. That said, we do not expect that the corrections to the spectral decomposition of those excited states would, as a byproduct, necessitate revisiting the value of the anisotropic exchange parameters \mathcal{J}_e . We are thus confident, combining the results presented in this paper and those of Ref. [16], that we have in hand the correct microscopic Hamiltonian of $\text{Yb}_2\text{Ti}_2\text{O}_7$ that includes all symmetry-allowed anisotropic bilinear nearest-neighbour couplings. One may therefore aim to proceed to unravel the nature of the low temperature ($T \lesssim 2$ K) state of this exotic material. In this context, it is worth commenting on the validity of the mean field theory treatment of our model at low temperatures ($T \lesssim 2$ K) and/or in weak field. Mean field theory predicts a transition to a $q = 0$ structure at approximately 1.1 K [16]. This contrasts with the experimental $T_c = 240$ mK [12]. As usual, mean field calculations neglect the effects of both thermal and quantum fluctuations. These could be fairly large in this system and greatly decrease the critical temperature. The role of thermal and quantum

fluctuations in the proposed Hamiltonian $H = H_{\text{int}} + H_{\text{cf}}$ for $\text{Yb}_2\text{Ti}_2\text{O}_7$ remains to be investigated. To the best of our knowledge, and notwithstanding the difficulties with mean field theory, the sharp specific heat feature signaling a phase transition in $\text{Yb}_2\text{Ti}_2\text{O}_7$ has only been reported in powder samples. It would be useful to confirm the existence of this feature in single crystals.

Two interesting observations that arise from this work are that (i) the isotropic exchange \mathcal{J}_{iso} is ferromagnetic (positive) in $\text{Yb}_2\text{Ti}_2\text{O}_7$ while it is found to be antiferromagnetic (negative) for the other $A_2\text{Ti}_2\text{O}_7$ compounds and (ii) there appears to exist large antisymmetric anisotropic exchange, described above in terms of the form of a Dzyaloshinskii-Moriya (DM) interaction. Very recent theoretical work [11] has found that large anisotropic exchange, including large DM interactions, can in principle arise in $\text{Yb}_2\text{Ti}_2\text{O}_7$. It would be interesting to investigate this issue further.

The conclusion of this work, that the magnetic exchange interactions in $\text{Yb}_2\text{Ti}_2\text{O}_7$ are anisotropic, hints at the possibility of significant multipolar interactions [10, 25] in this material and, perhaps, in other rare earth pyrochlores. That said, since the crystal field gap is much larger in $\text{Yb}_2\text{Ti}_2\text{O}_7$ than the scale of the interactions, anisotropic bilinear couplings between the \mathbf{J}_i operators as well as multipolar couplings between the Yb^{3+} moments manifest themselves, at low energies, in the form of generally anisotropic bilinear exchange couplings between effective pseudospins one-half [11].

Acknowledgments

We thank Shigeki Onoda for useful and stimulating discussions. This research was funded by the NSERC of Canada and the Canada Research Chair program (M. G., Tier I).

Appendix A. Previous works on local susceptibility in $\text{Yb}_2\text{Ti}_2\text{O}_7$

In this Appendix we discuss the anisotropic exchange fits of Refs. [8], for $\text{Yb}_2\text{Ti}_2\text{O}_7$, and [9] for various rare earth pyrochlore titanates.

The fit to χ_a presented in Ref. [8] and reproduced in Fig. 2b is based on a self-consistent mean field theory that considers a single sublattice. The moment $\langle \mathbf{J} \rangle$, at a temperature T , was computed from a mean field Hamiltonian consisting of the crystal field, a Zeeman term, and a mean field term arising from the interactions of the form $-g_J \mu_B \lambda_\alpha^C \langle J_\alpha \rangle$, where α specifies the components \parallel and \perp , the directions parallel and perpendicular to the local [111] direction. Solving for the moment, the two couplings λ_\parallel and λ_\perp were determined from a fit to χ_a . Since this model fails to take into account the sublattice structure of the pyrochlore lattice, the ensuing fit is unlikely to correctly reflect the underlying microscopic couplings in $\text{Yb}_2\text{Ti}_2\text{O}_7$.

The model of Ref. [9] includes the crystal field anisotropy as well as nearest neighbour exchange couplings and the long range dipole interaction (treated via an Ewald summation). The model correctly handles the sublattice structure of the

pyrochlore lattice. The model includes, at the outset, three exchange couplings which respect the lattice symmetries and which are denoted: $\lambda_{\perp,1}^M$, $\lambda_{\perp,2}^M$ and λ_{\parallel}^M . These can be expressed in terms of the couplings \mathcal{J}_e as follows:

$$\lambda_{\perp,1}^M = \frac{1}{3}\mathcal{J}_{\text{Ising}} + \mathcal{J}_{\text{iso}} + \mathcal{J}_{\text{pd}} \quad (\text{A.1})$$

$$\lambda_{\perp,2}^M = \mathcal{J}_{\text{iso}} + \frac{1}{2}\mathcal{J}_{\text{pd}} \quad (\text{A.2})$$

$$\lambda_{\parallel}^M = -\frac{2}{3}\mathcal{J}_{\text{Ising}} + \mathcal{J}_{\text{iso}} - 2\mathcal{J}_{\text{pd}} \quad (\text{A.3})$$

This set of couplings does not include the Dzyaloshinskii-Moriya coupling, \mathcal{J}_{DM} . Furthermore, in the fits to χ_a , Ref. [9] imposes the constraint $\lambda_{\perp,1}^M = \lambda_{\perp,2}^M$. While this choice most likely circumvents the problem of having an underconstrained set of couplings to fit the χ_a data, the reduction of the parameter space to a particular two dimensional surface within a four dimensional space of couplings appears to us to be somewhat arbitrary. Indeed, the couplings we have obtained from neutron scattering data and which we used in our fit to χ_a do not lie within the parameter space considered in Ref. [9]. For example, $\mathcal{J}_{\text{DM}} = -0.25$ K for our model with crystal field parameters taken from Ref. [8] (see Eq. 2), which is of the same order of magnitude as the other three couplings. Reference [9] makes use of their model to study the exchange couplings of a number of rare earth pyrochlore titanates finding a significant degree of anisotropy in the exchange in a number of cases. For the case of $\text{Yb}_2\text{Ti}_2\text{O}_7$, which is relevant to this article, they mention couplings that are much larger than those of the other materials considered but do not report these couplings.

References

- [1] Gardner J S, Gingras M J P, and Greedan J E 2010 Magnetic pyrochlore oxides *Rev. Mod. Phys.* **82**, 53.
- [2] Bramwell S T and Gingras M J P 2001 Spin Ice State in Frustrated Magnetic Pyrochlore Materials *Science* **294**, 1495.
- [3] Gardner J S *et al.* 2002 Co-operative Paramagnetism in the Geometrically Frustrated Pyrochlore, $\text{Tb}_2\text{Ti}_2\text{O}_7$ *Phys. Rev. Lett.* **82**, 1012.
- [4] Gingras M J P, Stager C V, Raju N P, Gaulin B D, and Greedan J E 1997 Static Critical Behavior of the Spin-Freezing Transition in the Geometrically Frustrated Pyrochlore Antiferromagnet $\text{Y}_2\text{Mo}_2\text{O}_7$ *Phys. Rev. Lett.* **78**, 947.
- [5] Chapuis Y, Dalmas de Réotier P, Marin C, Yaouanc A, Forget A, Amato A, and Baines C 2009 Probing the ground state of $\text{Gd}_2\text{Sn}_2\text{O}_7$ through μSR measurements *Physica B* **404** 686.
- [6] Lago J *et al.* 2005 Magnetic ordering and dynamics in the XY pyrochlore antiferromagnet: a muon-spin relaxation study of $\text{Er}_2\text{Ti}_2\text{O}_7$ and $\text{Er}_2\text{Sn}_2\text{O}_7$ *J. Phys.: Condens. Matter* **17** 979.
- [7] Bonville P *et al.* 2004 Transitions and spin dynamics at very low temperature in the pyrochlores $\text{Yb}_2\text{Ti}_2\text{O}_7$ and $\text{Gd}_2\text{Sn}_2\text{O}_7$ *Hyperfine Interactions* **156**, 103.
- [8] Cao H, Gukasov A, Mirebeau I, Bonville P, Decorse C, and Dhaleenne G 2009 Ising versus XY Anisotropy in Frustrated $\text{R}_2\text{Ti}_2\text{O}_7$ Compounds as Seen by Polarized Neutrons *Phys. Rev. Lett.* **103**, 056402.
- [9] Malkin B Z, Lummen T T A, van Loosdrecht P H M, Dhaleenne G, and Zakirov A R 2010 Static magnetic susceptibility, crystal field and exchange interactions in rare earth titanate pyrochlores *J. Phys.: Condens. Matter* **22**, 276003.
- [10] Onoda S, and Tanaka Y 2011 Quantum fluctuations in the effective pseudospin-1/2 model for magnetic pyrochlore oxides arXiv:1011.4981

- [11] Onoda S 2010 Effective quantum pseudospin-1/2 model for Yb pyrochlore oxides arXiv:1101.1230
- [12] Hodges J A *et al.* 2002 First-Order transition in the spin dynamics of geometrically frustrated $\text{Yb}_2\text{Ti}_2\text{O}_7$ *Phys. Rev. Lett.* **88**, 077204.
- [13] Y. Yasui *et al.*, *J. Phys. Soc. Jpn.* **72**, 3014 (2003).
- [14] Gardner J S, Ehlers G, Rosov N, Erwin R W, and Petrovic C 2004 Spin-spin correlations in $\text{Yb}_2\text{Ti}_2\text{O}_7$: A polarized neutron scattering study *Phys. Rev. B* **70**, 180404.
- [15] Ross K A, Ruff J P, Adams C P, Gardner J S, Dabkowska H A, Qiu Y, Copley J R, Gaulin B D 2009 Two-dimensional kagome correlations and field induced order in the ferromagnetic XY pyrochlore $\text{Yb}_2\text{Ti}_2\text{O}_7$ *Phys. Rev. Lett.* **103** 227202.
- [16] Thompson J D, McClarty P A, Rønnow H M, Regnault L-P, Sørge A, and Gingras M J P 2010 Rods of Neutron Scattering Intensity in $\text{Yb}_2\text{Ti}_2\text{O}_7$: Compelling Evidence for Significant Anisotropic Exchange in a Magnetic Pyrochlore Oxide arXiv:1010.5476.
- [17] Hodges J A, Bonville P, Forget A, Rams M, Królás K, and Dhaleenne G 2001 The crystal field and exchange interactions in $\text{Yb}_2\text{Ti}_2\text{O}_7$ *J. Phys. Condens. Matter* **13**, 9301.
- [18] McClarty P A, Curnoe, S H, and Gingras M J P 2009 Energetic selection of ordered states in a model of the $\text{Er}_2\text{Ti}_2\text{O}_7$ frustrated pyrochlore XY antiferromagnet *J. Phys.: Conference Series* **145**, 012032.
- [19] Elhajal M, Canals B, Sunyer R, and Lacroix C 2005 Ordering in the pyrochlore antiferromagnet due to Dzyaloshinsky-Moriya interactions *Phys. Rev. B.* **71**, 094420.
- [20] The measurements that have been made of the Curie-Weiss temperature [17, 26] all lie in the range 0.65 ± 0.15 K.
- [21] Onose Y, Ideue T, Katsura H, Shiomi Y, Nagaosa N, and Tokura Y 2010 Observation of the Magnon Hall Effect *Science* **329**, 297
- [22] Chern Gia-Wei, Fennie C J, and Tchernyshyov O 2006 Broken parity and a chiral ground state in the frustrated magnet CdCr_2O_4 *Phys. Rev. B* **74**, 060405
- [23] Gukasov A and Brown P J 2002 Determination of atomic site susceptibility tensors from polarized neutron diffraction data *J. Phys.: Condens. Matter* **14** 8831
- [24] Enjalran M and Gingras M J P 2004 Theory of paramagnetic scattering in highly frustrated magnets with long-range dipole-dipole interactions: The case of the $\text{Tb}_2\text{Ti}_2\text{O}_7$ pyrochlore antiferromagnet *Phys. Rev. B* **70**, 174426.
- [25] Santini P *et al.* 2009 Multipolar interactions in f-electron systems: The paradigm of actinide dioxides *Rev. Mod. Phys.* **81** 807
- [26] Bramwell S T *et al.* 2000 *J. Phys.: Condens. Matter* **12** 483.